CrystEngComm

Accepted Manuscript

ROYAL SOCIETY OF CHEMISTRY

www.rsc.org/crystengcomm

OPTICAL AND SPECTROSCOPIC STUDIES OF $Ca_{0.9}Nd_{0.1}Ti_{0.9}Al_{0.1}O_3$ SINGLE CRYSTALS GROWN BY OPTICAL FLOATING ZONE TECHNIQUE

G. Murugesan, R. Nithya[a], S. Kalainathan* and T.R. Ravindran[a]

Centre for Crystal Growth, School of Advanced Sciences, VIT University, Vellore 632 014, Tamil Nadu, India

[a]*Materials Science Group, Indira Gandhi Centre for Atomic Research, Kalpakkam 603 102, Tamil Nadu, India*

***Corresponding author**
Prof.S.Kalainathan
VIT University, Vellore - 632014, Tamilnadu, India.
Phone: +91-416-2202350, Fax: 0416-2243092
E-mail Address: kalainathan@yahoo.com

Abstract

Single crystals of multifunctional $Ca_{0.9}Nd_{0.1}Ti_{0.9}Al_{0.1}O_3$ have been grown in air and also in argon atmosphere using optical float zone technique. The phase composition of the grown single crystal was verified by powder X-ray diffraction technique. Quality of the grown single crystals was ascertained by Rocking Curve and Laue patterns. Raman spectra showed the disordering in B cation site due to the valence mismatch between Ti^{4+} and Al^{3+}. The energy levels of Nd^{3+} in the $CaTiO_3$ matrix were determined using the absorption and emission spectra. An absorption band at 806nm and a strong emission band at 1064.48nm show that the crystal has good laser optical quality for diode-laser pumping.

1. Introduction

$CaTiO_3$ (CTO), a well-known perovskite that crystallizes in orthorhombic structure with space group Pbnm is used for phosphor materials [1], as a major phase in SYNROC which can immobilize Strontium (Sr), Barium (Ba), rare earths and long-lived actinides such as Plutonium (Pu) [2] and as dielectric resonators in wireless communication systems due to its high relative permittivity, variable temperature coefficient of resonant frequency and low dielectric loss [3]. Due to the similar ionic radii of

Calcium (Ca^{2+}, CN-12: 0.134nm) and rare earth ions Praseodymium (Pr^{3+}, CN-9: 0.118nm), Neodymium (Nd^{3+}, CN-12: 0.127nm), $CaTiO_3$ is being used as a host for efficient strong red luminescence under UV excitation [4]. About 70% of Ca^{2+}cations in $CaTiO_3$ could be replaced by Nd^{3+}cations and doping Al^{3+} in Ti^{4+} site for charge compensation does not affect the crystal structure [5]. The structural compatibility of $CaTiO_3$ (orthorhombic) – $NdAlO_3$ (rhombohedral) based ceramics allows them to be used for commercial production of microwave dielectric resonators in wireless communications [5-6].

Due to versatile properties like high efficiency, compactness, cost-effective and stability, diode pumped solid-state lasers are being used in various applications like medical diagnostics, generation of terahertz radiation, spectral broadening of light (super-continuum), medical imaging (optical coherent tomography) [7-8]. Neodymium (Nd) doped single crystals exhibit higher laser output powers than glasses due to its thermo-mechanical and thermo-optical properties [7]. Nd doped single crystals are also used as sources of infrared radiation due to the strongest laser transition from $^4F_{3/2}$ to $^4I_{11/2}$ which finds its way for various applications in the field of medicine, processing of materials, IR cameras and remote controls [1]. Presence of Nd in the crystal makes it a suitable candidate for solid state lasers. Nd substituted CTO compounds have been synthesized by different methods which includes: solid state reaction [6], complex polymerization [9], and sol-gel method [1]. There are only few reports about the spectroscopic properties of Nd doped $CaTiO_3$, Marques et al studied about the optical properties of $CaTiO_3$: Nd^{3+} powders [9], later on Lemanski et al first time discussed the luminescence properties of Nd^{3+} doped $CaTiO_3$ nanocrystals [1]. To our knowledge there are no reports for optical and spectroscopic properties of Nd^{3+} doped $CaTiO_3$ single crystals. Thus, we have grown Nd substituted $CaTiO_3$ single crystals using optical floating zone technique. We report in this study the difficulties in growing good quality $Ca_{0.9}Nd_{0.1}Ti_{0.9}Al_{0.1}O_3$ (CNTAO) single crystals and their optical, vibrational and luminescence properties.

2. Experimental details

High quality single crystals of $Ca_{0.9}Nd_{0.1}Ti_{0.9}Al_{0.1}O_3$ were grown by spontaneous nucleation using optical floating zone technique**.** High purity (4N) powders of $CaCO_3$, Nd_2O_3, TiO_2, Al_2O_3 were mixed in stoichiometric ratio by ball milling to obtain a homogenous powder. The powders were preheated to remove moisture at 700^{o}C for 10hrs. This mixture was calcined at 1200^{o}C for 10h in air with one intermediate grinding. After calcination the powders were ground once again and heated and this procedure was repeated till a single phase compound was formed. After confirmation of single phase by powder X-Ray diffraction (XRPD), the powders were packed and sealed into a rubber tube which was evacuated using a vacuum pump. The powders were then compacted into a rod using a hydraulic press under an isostatic pressure of 70 MPa. The length and dia of the pressed rods were 50mm and 7mm respectively. The pressed rods were sintered at 1300^{o}C for 12h in air.

Single crystals were grown from the feed and seed rods in a four mirror optical floating zone furnace (Crystal SystemsCorp.FZ-T-4000-H-HR-I-VPO-PC). The crystals were grown by counter rotating the seed and the feed rods at 20-30 rpm and the molten zone was translated upwards during crystal growth with a translation speed of 10-20 mm/h in air and also in argon atmospheres. The grown single crystals were cut in the form of discs perpendicular to the growth direction. Both sides of the disc were polished to a mirror finish. The diffraction data were recorded using Cu-K_α in the 2θ range of 10^o to 80^o. Laue diffraction (Philips diffractometer) and rocking curve analysis (Bruker D8 Discover) were carried out to check the crystalline perfection. Raman and luminescence spectra measurements were carried out using a Renishaw micro Raman spectrometer with 514& 488 nm laser excitations at ambient temperature. The absorption spectra of CNTAO single crystal were measured in the range 190-1100nm using ELICO 7b SL 218 double beam spectrophotometer. IR spectra were recorded from 4000cm^{-1}to 500 cm^{-1} using a FT-IR spectrometer (ABB make model MB3000) with a DTGS (deuterated triglycine sulphate) detector. Thermoluminescence measurements were carried out using a RISO TL/OSL reader (model DA-20) having an inbuilt 90Sr source with a dose rate of 60Gy. Brillouin scattering

measurements were performed on the (100) surface of the crystal in back-scattering geometry using a high-contrast 3 +3 pass Sandercock tandem Fabry-Perot interferometer. Didoe-pumped solid-state laser of wavelength 532nm was used as an excitation source.

3. RESULTS AND DISCUSSION

Shown in Figure 1 is the XRD pattern of CNTAO crushed single crystal powder and CNTAO powder which matches with the JCPDS data (#22-0153) confirming orthorhombic structure. It is also evident from the pattern that the starting materials and the grown crystal are of the same phase, no impurity peaks were observed after melting. Figure 2 shows the Rietveld refinement performed on the $Ca_{0.9}Nd_{0.1}Ti_{0.9}Al_{0.1}O_3$ crushed single crystal powder. Rietveld refinement was performed using GSAS program [10]. The Rietveld refinement results are presented in Table 1. The refined lattice parameters for orthorhombic CNTAO single crystal phase are a = 5.382514 A˚, b = 5.436576 A˚ and c = 7.640289 A˚ ($\alpha = \beta = \gamma = 90^o$). These Rietveld refinement results show that $CaTiO_3$ is a good host for Nd^{3+} where Nd^{3+} ions substitute Ca^{2+} sites while Al^{3+} ions replace Ti^{4+} sites.

When the crystal growth was initially carried out in air atmosphere (run 1), the molten zone was stable as shown in Figure 3(a) and as the growth proceeded the zone diameter started reducing as shown in Figure 3(b) & (c) and finally it got disconnected. The molten zone was stable for a few millimetres of growth only and again it started reducing and collapsed. The grown crystal in air atmosphere is shown in the Figure 3(d). Maintaining a stable zone in air atmosphere was found to be difficult. Thus we grew the crystal in argon atmosphere (run 2); the molten zone was quite stable when we performed the growth process in static argon atmosphere. When the crystal is grown in dynamic atmosphere of argon gas (run 3), we found the molten zone even more stable. The crystals grown in argon atmosphere are shown in Figure 4(a) & (b). The crystals were black in colour due to oxygen vacancies and became transparent after annealing them in oxygen atmosphere at 1000˚C. Optimized growth parameters of the grown crystals are summarized in Table 2.

In order to check the crystalline perfection, Laue pattern was obtained in both transmission and back reflection geometries, circular black spots with patterns were obtained which shows that the crystal is of good quality. Laue pattern form arbitrary plane of the CNTAO single crystal grown in argon atmosphere is shown in the Figure 4(c) & (d). Due to unavailability of goniometer with the cutting machine we were unable to cut the crystal in the desired plane, so we faced a difficulty in finding the orientation of the grown crystal by Laue pattern. In order to determine the plane of growth, we performed XRD measurements on cut disc of the crystal. The inset in Fig. 1 shows the diffraction pattern of as grown single crystal. We can see that the crystal is grown in 200 orientation. There were two and more peaks around the 200 and 400 Bragg reflections, which is due to the mosaic spread in the single crystal. This is confirmed by rocking curve analysis. High-resolution X-ray diffraction (HR-XRD) analysis was carried out, the diffraction pattern was recorded in parallel beam geometry. A well collimated Cu K_α beam obtained from a 6 kW rotating anode is directed to the sample via a Göbel mirror and 1mm slit. Figures 5 (a) & (b) show the high resolution X-ray diffraction patterns for 2 0 0 and 4 0 0 planes families of crystals grown in air. As seen in Figures 5 (a) & (b), the curve does not contain a single diffraction peak. The solid line (red colour) that follows well the experimental points (black filled circles), is the convoluted curve of two peaks fitted using Lorentzian fit. The presence of additional peaks at 27 & 73arc secs for 200 plane and 45 & 21 arc secs for 400 plane from the centre are due to internal structural low angle boundary which proves that the crystal grown in air is of poor quality [11]. The HR-XRD pattern of the crystal grown in argon atmosphere is shown in Figures 5 (c) and (d), the sample was rocked (ω-scan) around the peak corresponding to 200 and 400 plane families. The peaks are asymmetric which could be convoluted into two peaks as shown in the figure. The additional peak is due to the internal structural low angle boundary [11].The FWHM of the rocking curve is 24 and 19 arc secs which proves that crystal grown in argon atmosphere is better that of crystal grown in air atmosphere.

2.1 Raman spectroscopy

Substitution of Al^{3+} in Ti^{4+} for charge compensation, makes $CaTiO_3$ a complex perovskite (where Ti and Al are two different elements with different oxidation states), microscopic cationic arrangement of such complex materials brings about changes in vibrational spectra when compared with the pristine ABO_3 structure [12]. To probe the B-site ordering Raman scattering measurements were done on pure $CaTiO_3$ powder (prepared by solid state reaction) and CNTAO single crystals. Figure 6 shows Raman spectra measured on pure $CaTiO_3$ polycrystalline powder prepared by solid state reaction and CNTAO single crystal using 514nm and 488nm laser. Several first-order Raman bands in the wavenumber range 100 to 850 cm^{-1}were observed. In this orthorhombic unit cell there is one crystallographic position for Ca/Nd, one for Ti/Al and two for O ions. From group theoretical analysis using SAM module in Bilbao crystallographic server for orthorhombic structure with Pbnm symmetry, the calculated irreducible representation is

$$\Gamma_{Raman} = 7A_g + 5B_{1g} + 7B_{2g} + 5B_{3g}$$

From Figure 6 it is evident that 16 out of 24 Raman active modes were detected. Not all bands were detected in the Raman spectra due to overlap of some bands with other intense bands or due to insufficient intensity. Table 3 shows the Raman modes for pure and substituted $CaTiO_3$ measured with 514nm and 488nm. When the spectra were recorded using 514nm wavelength laser, we were able to observe Nd^{3+} emission lines at 545cm^{-1} which corresponds to $4I_{9/2}$ energy levels. In order to confirm Nd^{3+} emission lines the spectra were recorded using laser wavelength of 488nm. From the figure it is evident that modes around 176,218,241, 282 and 335 cm^{-1} correspond to O-Ti-O bending modes, 464 and 500 cm^{-1} are associated to Ti-O_3 torsional (bending or internal vibration of the oxygen cage) modes [13-17]. The broad mode around 790 $cm^{-1}$is absent in pure $CaTiO_3$, but present in CNTAO spectra suggesting that this mode is related to cation disorder/order (A_{1g} mode) which is usually observed in complex perovskites [12, 18-19]. Presence of A_{1g} oxygen breathing mode is due to the substitution of Al^{3+} in Ti^{4+}sites which

brings about disorder. The width of A_{1g} mode reflects the degree of order, smaller the width higher the degree of order and vice versa [12]. In our case the widths of the A_{1g} mode is much higher proving the degree of disorder is higher.

2.2 Absorption and Emission characteristics

To record absorption spectra, the crystal was polished to 0.7 mm thickness. Figure7 shows the absorption spectrum for CNTAO single crystal consisting of several sharp absorption lines corresponding to the stark levels of neodymium in CNTAO single crystal. The absorption coefficient was calculated using the following relation:

$$\alpha = \frac{2.303 \log\left(\frac{1}{T}\right)}{t} \qquad (1)$$

where α is the absorption coefficient, T is the transmittance which is calculated from absorption spectrum and t is the thickness of the crystal. The optical band gap of the grown CNTAO single crystal is evaluated from the absorption coefficient (α) using the relation:

$$\alpha h\nu = A\left(h\nu - E_g\right)^k \qquad (2)$$

where E_g is the optical band gap, A is a constant, ν is the frequency of incident photons and h is the Planck's constant, k is a constant associated with the different types of electronic transitions. Following Marques et al [9], $Ca_{0.99}Nd_{0.01}TiO_3$ (CNT) are characterized by indirect allowed electronic transition with value of k = 2. Thus, the E_{gap} values were determined by extrapolating the linear portion of the curve in the absorbance spectra. Using Tauc's method [20], the graph (Fig. 8) has been plotted for the product of absorption coefficient (α) and incident photon energies. The band gap estimated is 3.05 eV for the grown crystal. The energy band gap for CNT powders is 3.46eV [9], but for CNTAO single crystal it is around 3.05 eV which is due to the contribution of Nd 4f electrons which are closer to the lower edge of the conduction band resulting in the formation of new lowest unoccupied molecular orbits [21]. This suggests that co-substitution of Nd^{3+} and Al^{3+} has influenced the band gap of $CaTiO_3$.

Absorption band corresponding to the $4I_{9/2} \rightarrow 4F_{5/2} + 2H_{9/2}$ at 806 nm due to Nd^{3+} absorption transition in the CNTAO crystal shows that this crystal can be used for diode pumping [7, 22].The luminescence spectrum recorded in the IR region using excitation wavelength of 785 nm is shown in Fig.9 (a).The peaks were fitted using Lorentz function, the strong peak at 1064.48 nm due to $4F_{3/2} \rightarrow 4I_{11/2}$ Nd^{3+} emission transition also shows that the grown single crystal has good laser optical quality for diode-laser pumping [7, 22]. The stark energy levels ofNd^{3+} in CNTAO single crystal obtained from the absorption spectrum in the UV-VIS-IR region and emission spectrum (Figure 9(b)) are listed in Table 4.

In order to obtain information about the trapping centres, thermo-luminescence spectra were recorded. Figure 10 shows the TL glow curves for the grown CNTAO single crystal. This is the first report of the TL glow curve for this material. The TL peak is asymmetric which can be de-convoluted into two curves at 158˚C and 271˚C. The presence of two different thermal peaks indicates that there are two traps existing in the single crystal. The major trap which stores the photo-excitation energy is associated with the thermal peak at 271˚C. The other trap corresponds to a thermal peak at 158˚C. Pure $CaTiO_3$ has a trapping centre around 169˚C [24]. The thermal peak at 271˚C corresponds to Nd^{3+} emissions [25].

Acoustic velocities of the materials could be determined from the frequency shift of light scattered from thermally generated acoustic waves using Brillouin scattering [26]. Our crystals are transparent after annealing in oxygen atmosphere. We performed Brillouin scattering experiment on our transparent, colourless, unstrained single crystals with mirror-polished surface. Figure11shows the Brillouin spectrum of CNTAO single crystal, which consists of a Brillouin doublet arising from the longitudinal acoustic mode (LA) and transverse acoustic mode (TA) at about 57 GHz and 15 GHz respectively. The spectrum showed sharp peaks which proves that the grown single crystal is of high-quality [27].

3. Conclusion

Good quality single crystals of $Ca_{0.9}Nd_{0.1}Ti_{0.9}Al_{0.1}O_3$ were grown in argon atmosphere, quality of the crystal was ascertained by Laue diffraction spots and rocking curve analysis. The refinement results show that $CaTiO_3$ is a good host for Nd^{3+} substitution. The absorption bands of Nd^{3+}around 806nm corresponding to the $4I_{9/2} \longrightarrow 4F_{5/2} + 2H_{9/2}$ transition and emission bands around 1064nm corresponding to $4F_{3/2} \longrightarrow 4I_{11/2}$ emission transition prove that the crystal has good optical quality for diode-laser pumping. Nd^{3+} emissions were observed in Raman measurements using 514nm wavelength laser source, in order to confirm this measurements were done using 488nm wavelength laser source. Presence of A_{1g} oxygen breathing mode was observed in CNTAO grown single crystal proving it to be a complex pervoskite.

ACKNOWLEDGEMENTS:

GM thanks UGC-DAE Consortium for Scientific Research for providing a financial support and VIT University management for their constant encouragement. This work has been carried out at UGC-DAE Consortium for Scientific Research, Kalpakkam Node, Kokilamedu. We thank Dr. D. Sornadurai (MSG-IGCAR) for Laue photographs, Dr.SujoyChakravarty (UGC-DAE Constorium for Scientific Research, Kalpakkam Node) for rocking curve measurements, Dr.U. Madhusoodanan (IGCAR, Kalpakkam) for Thermoluminescence measurements and Dr.V. Sivasubramanian for Brillouin scattering measurement.

References:

1. K. Lemanski, A.Gagor, M.Kurnatowska, R.Pazik, P.J.Deren, Journal of Solid State Chemistry 184 (2011) 2713–2718.
2. Rodney C. Ewing, Progress in Nuclear Energy, 49 (2007), 635-643.

3. Bostjan Jancar, Danilo Suvorov, Matjaz Valant, Goran Drazic, Journal of the European Ceramic Society 23 (2003) 1391–1400.
4. P.J. Dere´n, R. P¸azik, W. Str¸ek, Ph. Boutinaud, R. Mahiou, Journal of Alloys and Compounds 451 (2008) 595–599.
5. E.R. Kipkoech, F. Azough, R. Freer, C. Leach, S.P. Thompson, C.C. Tang, Journal of the European Ceramic Society 23 (2003) 2677–2682.
6. Bostjan Jancar, Matjaz Valant, and Danilo Suvorov, Chem. Mater. 2004, 16, 1075-1082.
7. L B Su, Q G Wang, H J Li, G Brasse, P Camy, J L Doualan, A Braud, R Moncorg´e, Y Y Zhan, L H Zheng, X B Qianand J Xu, Laser Phys. Lett. 10 (2013) 035804.
8. Jin Zhu, Fulan Zhong, Naifeng Zhuang, Jianzhong Chen, Materials Letters 61 (2007) 374–379.
9. V.S. Marques, L.S. Cavalcante, J.C. Sczancoski, E.C. Paris, J.M.C. Teixeira, J.A. Varela, F.S. De Vicente, M.R. Joya, P.S. Pizani, M. Siu Li, M.R.M.C. Santos, E. Longo, Spectrochimica Acta Part A 74 (2009) 1050–1059.
10. A.C. Larson and R.B. Von Dreele, General Structure Analysis System (GSAS), Los Alamos National Laboratory Report LAUR 86-748 (2004).
11. G. Bhagavannarayana, R. V. Ananthamurthy, G. C. Budakoti, B. Kumar and K. S. Bartwal, J. Appl. Cryst. (2005). 38, 768–771.
12. I. G. Siny, R. S. Katiyar and A. S. Bhalla, Journal of Raman Spectroscopy, Vol. 29, 385È390 (1998).
13. U. Balachandran and N.G. Eror, Solid State Communications, Vol. 44, No. 6, pp. 815-818, 1982.
14. Shan Qin, XiangWu, Friedrich Seifert and Ana I. Becerro**,** J. Chem. Soc., Dalton Trans., 2002, 3751–3755.
15. Mario L. Moreira, Elaine C. Paris, Gabriela S. do Nascimento, Valeria M. Longo,Julio R. Sambrano, Valmor R. Mastelaro, Maria I.B. Bernardi, Juan Andre´s, Jose´ A. Varela, Elson Longo, Acta Materialia 57 (2009) 5174–5185.

16. Yuan Li, Shan Qin, Friedrich Seifert, Journal of Solid State Chemistry 180 (2007) 824–833.
17. Mael Guennou, Pierre Bouvier, Benjamin Krikler, and Jens Kreisel, Phys. Rev. B 82, 134101 (2010).
18. H. Zhenga, G.D.C. Csete de Gyorgyfalva, R. Quimbya, H. Bagshawa, R. Ubicb, I.M. Reaneya, J. Yarwoodc, Journal of the European Ceramic Society 23 (2003) 2653–2659.
19. Chun-Hai Wang and Xi-Ping Jing, J. Am. Ceram. Soc., 92 [7] 1547-1551 (2009).
20. D.L. Wood, J. Tauc, Phys. Rev. B 5 (1972) 3144-3152.
21. W. Li, Y. Wang, H. Lin, S. Ismat Shah, C. P. Huang, D. J. Doren, Sergey A. Rykov, J. G. Chen and M. A. Barteau, Appl. Phys. Lett., Vol. 83, No. 20.
22. Mingfu Zhang, Huaixin Guo, Jiecai Han, Hailiang Zhang, Chenghai Xu, Journal of Crystal Growth 340 (2012) 130–134.
23. P. J. Dereń,A. Bednarkiewicz,Ph. Goldnerand O. Guillot-Noël, J. Appl. Phys. 103, 043102 (2008).
24. M. Shivaram, R. Hari Krishna, H. Nagabhushana, S.C. Sharma, B.M. Nagabhushana, B.S. Ravikumar, N. Dhananjaya, C. Shivakumara, J.L. Rao, R.P.S. Chakradhar, Materials Research Bulletin 48 (2013) 1490–1498.
25. Ya. Zhydachevskii, I.I. Syvorotka , L. Vasylechko, D. Sugak,I.D. Borshchyshyn, A.P. Luchechko,Ya.I. Vakhula, S.B. Ubizskii , M.M. Vakiv, A. Suchocki, Optical Materials 34 (2012) 1984–1989.
26. S. Mitra, High pressure Geochemistry and Mineral Physics PP 368, Elsiever (2004).
27. Carmen Sanchez-Valle, Stanislav V. Sinogeikin, Joseph R. Smyth and Jay D. Bass, American Mineralogist, Volume 91, PP 961-964, 2006.

Tables and Figures:

Table 1.Rietveld refinement results and atomic coordinates used to depict the CNTAO single crystal unit cell.

Atom	Site	X	y	z
Ca/Nd	4c	-0.008458	0.031675	0.25
Ti/Al	4b	0	0.5	0
O1	4c	0.054403	0.489425	0.25
O2	8d	0.720047	0.285046	0.034367

Space group Pbnm, $\chi^2 = 2.761$, $R_p = 14.85$, $R_{wp} = 19.15$, Temp: 27^{o}C

Table 2. Growth parameters of CNTAO crystals

Growth parameters	RUN 1	RUN 2	RUN 3
Growth rate (mm/h)	10	10-20	10-20
Rotation rate (rpm)	20-30	20-30	20-30
Ambience	Air	Argon(static flow)	Argon (dynamic flow)
Pressure (atm)	Nil	3.5 bar	3.5 bar

Table 3. Raman-active modes for CNTAO single crystal and $CaTiO_3$ polycrystalline material.

	$CaTiO_3$ (Polycrystalline)	CNTAO (Single crystal)	CNTAO (Single crystal)	Raman modes [17]
Laser source wavelength	514nm	514nm	488nm	
Synthesis process	Solid state reaction	Optical floating zone technique	Optical floating zone technique	
Ca-TiO_3 lattice mode	146	150	146	B_{2g}
O-Ti-O bending mode	176	178	176	B_{1g}
O-Ti-O bending mode	221	221	218	B_{1g}
O-Ti-O bending mode	241	244	241	A_g
O-Ti-O bending mode	281	285	282	A_g
O-Ti-O bending mode	333	329	335	A_g
Ti-O_3 torsional mode	463	470	464	A_g
Ti-O_3 torsional mode	498	----	500	A_g
Nd emission	----	546	----	----
Ti-O symmetry stretching	----	----	661	----
Oxygen breathing mode	----	790	785	A_{1g}

Table 4. Comparative results of energy levels of Nd^{3+} ions in CNTAO single crystal assigned from the absorption and emission spectra with those reported in literatures.

	Energies (cm^{-1})		
Level of Nd^{3+}	This work	$CaTiO_3$: Nd^{3+}Nano powders [1]	$LaAlO_3$: Nd^{3+} single crystal [23]
$^4I_{11/2}$	2018, 2074, 2119,2215	1928,2027,2083,2130,2225,2285	2069, 2078, 2168, 2255, 2286, 2332
$^4I_{13/2}$	3948.7	3966, 4063, 4148, 4266, 4380	3977, 4041, 4099, 4169, 4256, 4286, 4357
$^4F_{3/2}$	11406,11512	11409, 11512	11 583, 11 619
$^4F_{5/2} + {}^2H_{9/2}$	12518,12684,12831,12963	12242, 12300, 12326, 12386, 12447, 12497, 12536	12 547, 12 553, 12 627, 12 645, 12 658, 12 813, 12 822
$^4S_{3/2}$	13425,13567	13337, 13442	13 452, 13 566
$^4F_{9/2}$	14558	14630	14 831, 14 859, 14 908, 14 914, 14 918
$^2H_{11/2}$	15877,15953,16513	15610, 15943	15 969, 16 012, 16 074, 16 168
$^4G_{5/2} + {}^2G_{7/2}$	17011,17154, 17274, 17422	16976, 17270	17 098, 17 130, 17 142, 17 321, 17 487, 17 495, 17 540
$^4G_{7/2} + {}^4G_{9/2}$	18907,19038, 19382	18401, 18915, 19350	18 947, 18 973, 19 036, 19 047, 19 147, 19 180, 19 235, 19 274, 19 330
$^2K_{13/2}$	19522	-------	19 523, 19 531, 19 549, 19 531, 19 655, 19 667, 19 737
$^2G_{9/2}$	20879	-------	20 166, 20 310, 20 451, 20 592, 20 747, 20 878
$^2P_{1/2}$	23149	23388	23 349
$^2D_{5/2}$	23961,23965	--------	23 906, 23 946, 23 980
$^2P_{3/2}$	25420,25614	--------	26 221, 26 257
$^2I_{11/2}$	29176	--------	28 484, 28 573, 28 655, 28 707, 29 225, 29 247
$^4D_{7/2}$	29990, 30249, 30434	--------	30 052, 30 155, 30 341

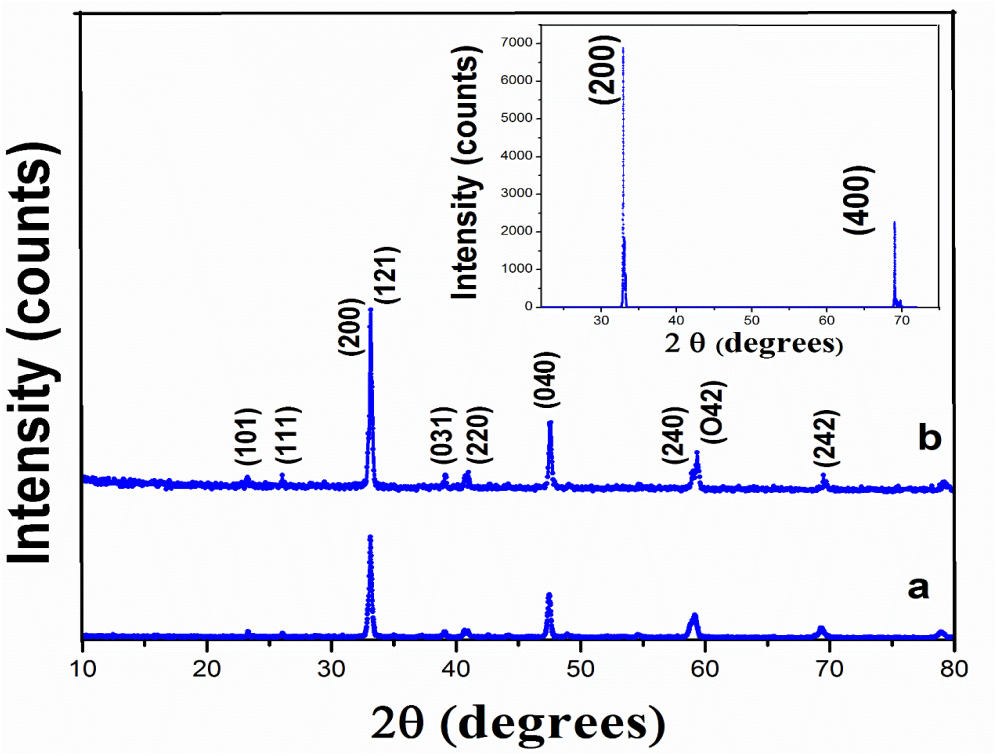

Figure 1. Powder XRD patterns of (a) Polycrystalline and (b) Crushed single crystal of CNTAO. Inset shows the diffraction of as grown (200) oriented single crystal.

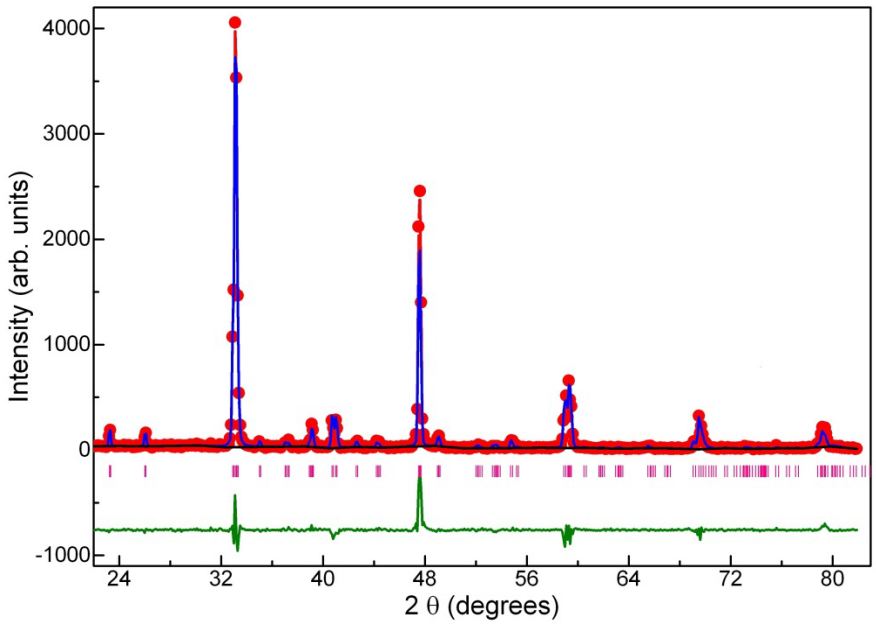

Figure 2. Rietveld refinement of crushed CNTAO single crystal powder.

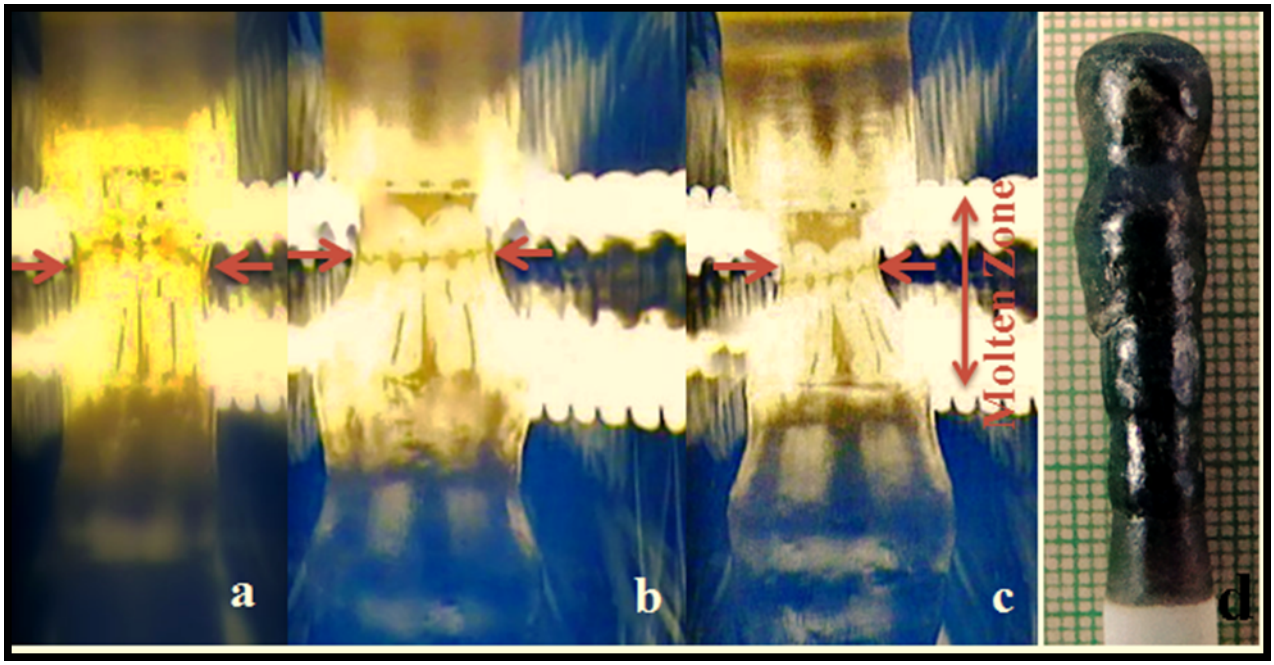

Figure 3. (a-c) Molten zone images during CNTAO (run1) in air atmosphere. d. CNTAO grown crystal in air atmosphere

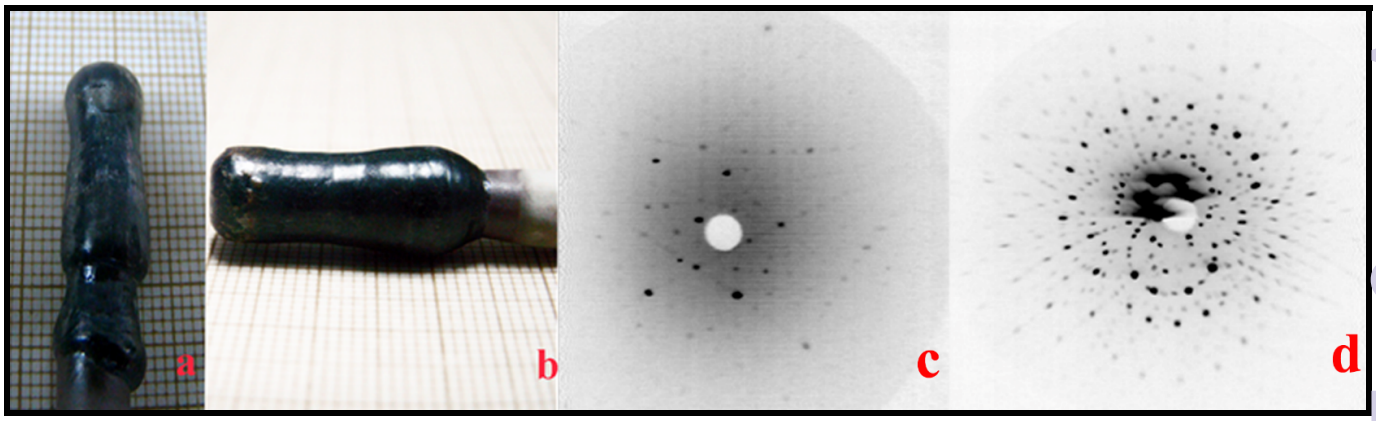

Figure 4. Photographs of single crystals of CNTAO grown in argon atmosphere (a- static growth and b- dynamic growth), (c) back scattered and (d) transmission Laue diffraction patterns (run 3).

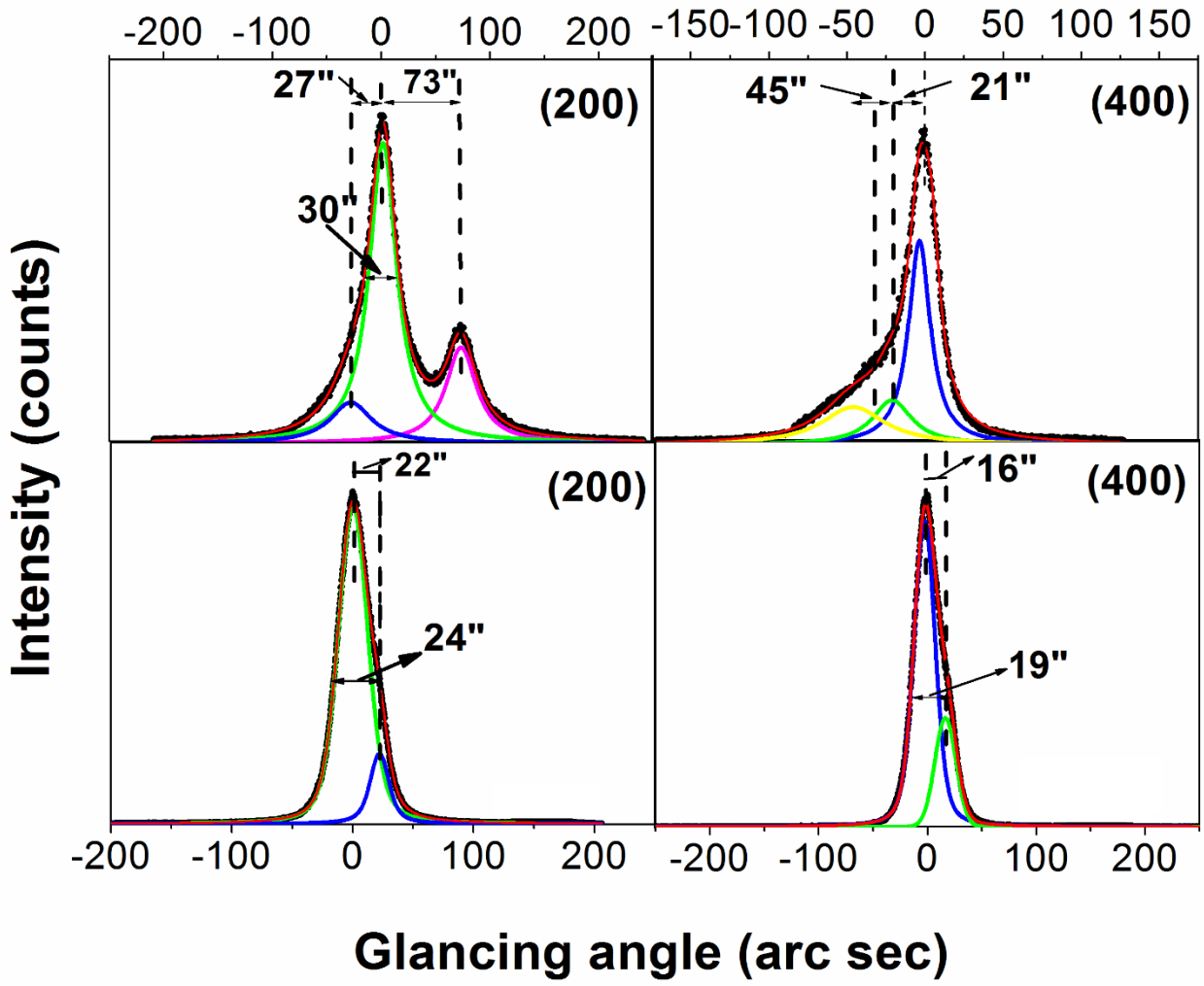

Figure 5. (a) & (b) Rocking Curves for CNTAO crystals grown in air atmosphere, (c) & (d) crystal grown in argon atmosphere for (200) and (400) diffracting planes using Cu K_α radiation.

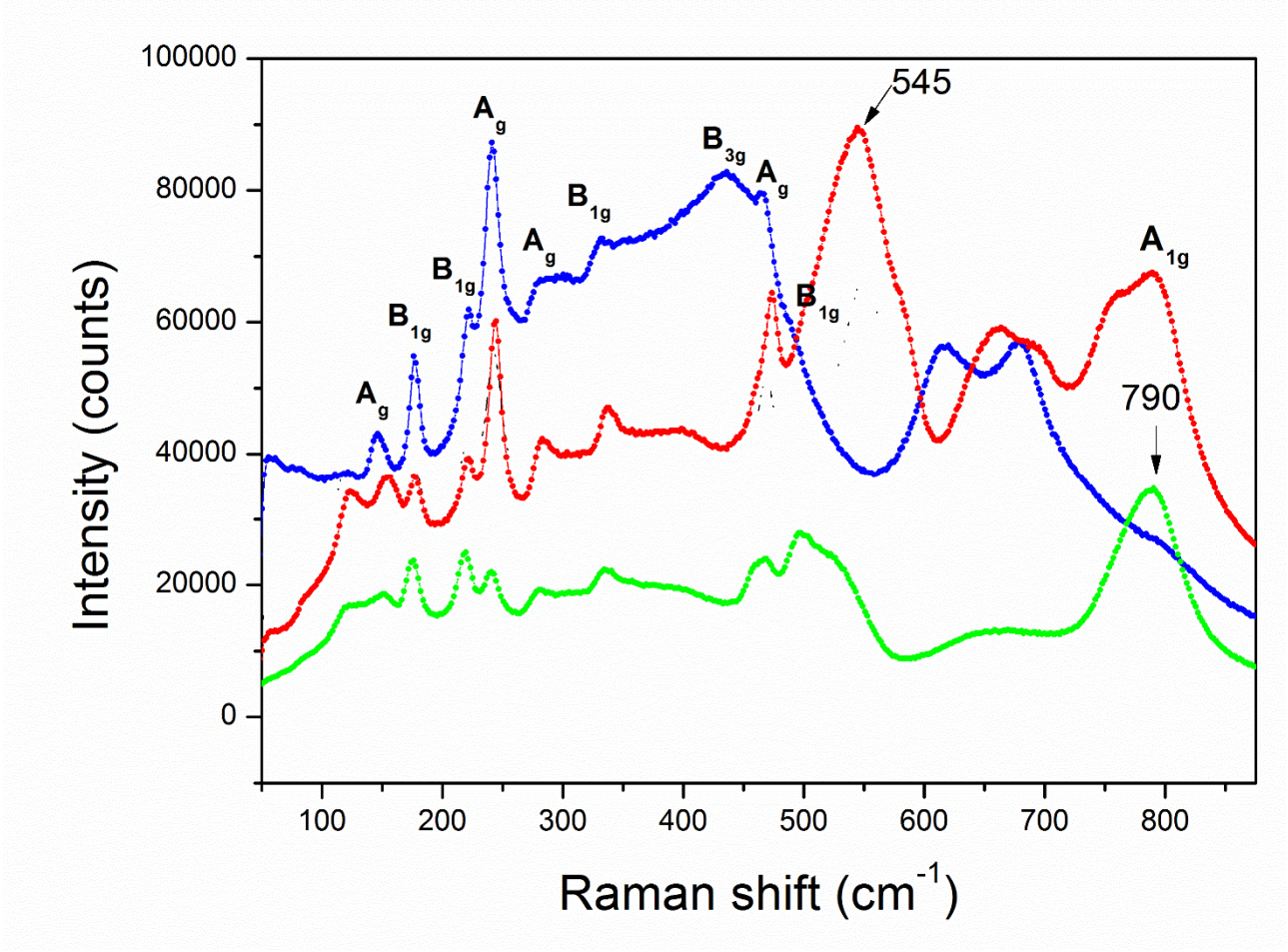

Figure 6. Raman spectra of (a) Polycrystalline $CaTiO_3$, (b) grown CNTAO single crystal using 514nm laser source (c) 488nm laser source.

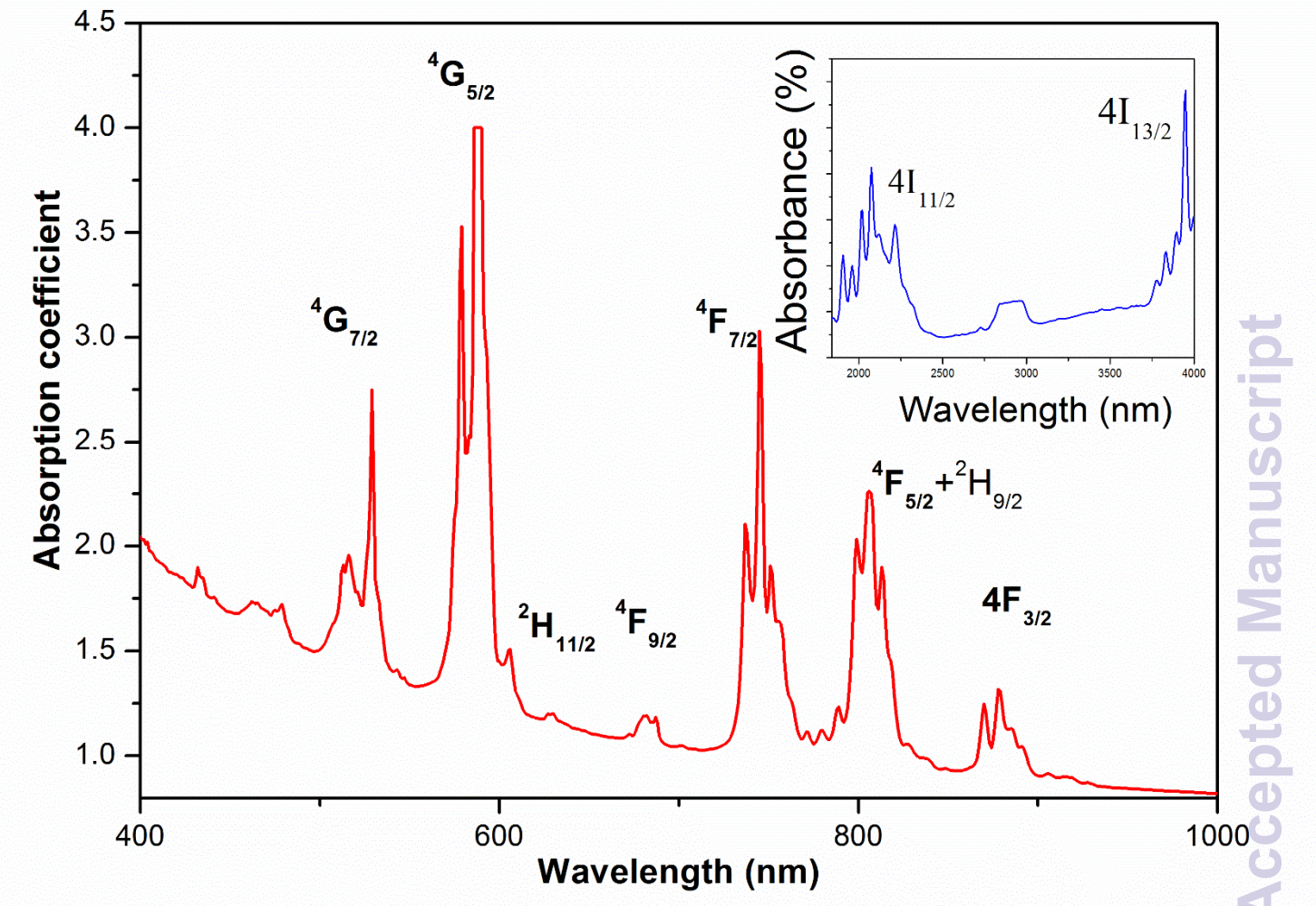

Figure 7. Absorption spectra of the grown single crystal measured in the UV-VIS-NIR range. Inset shows the absorption spectra recorded in the IR range.

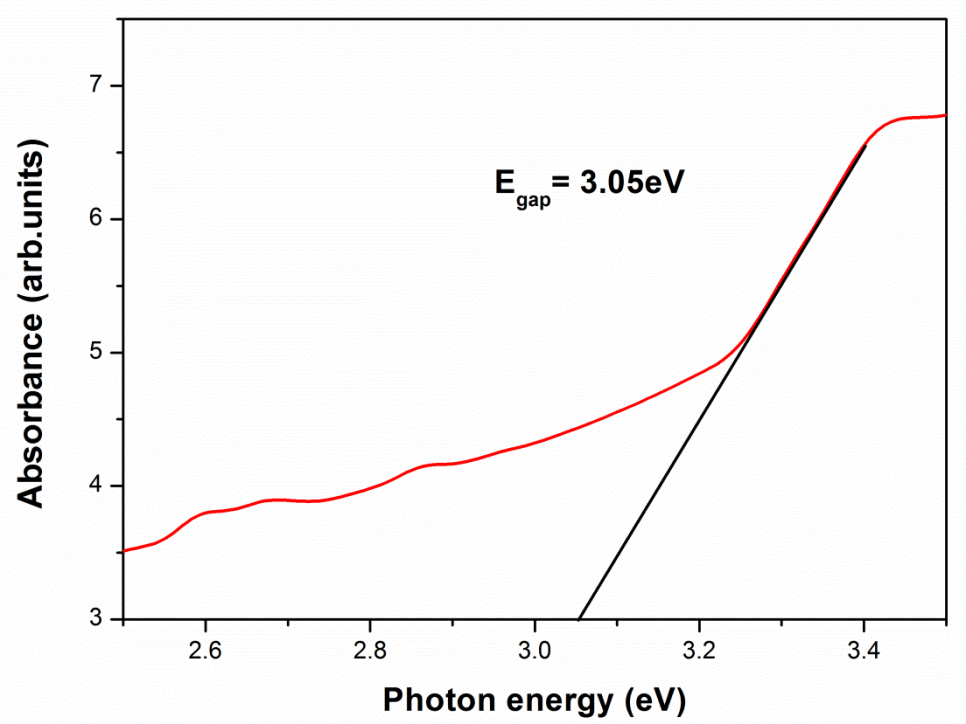

Figure 8.Plot of absorbance of CNTAO single crystal as a function of photon energy.

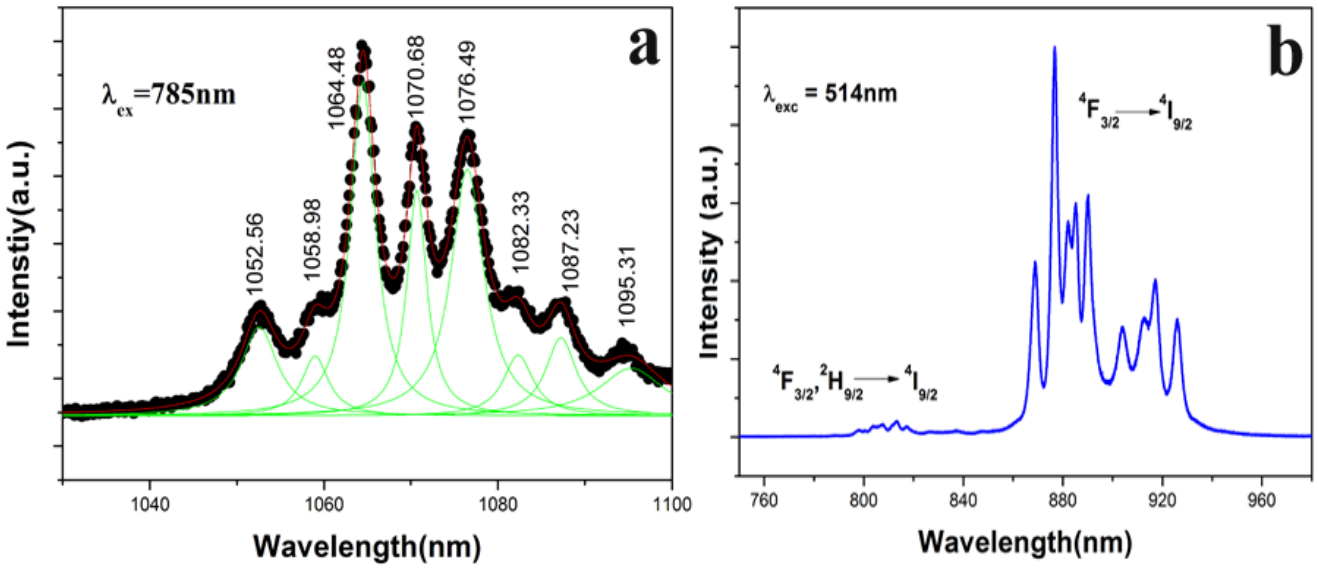

Figure 9.Photo-luminescence spectra for CNTAO single crystal excited at (a) 785nm (b) 514 nm.

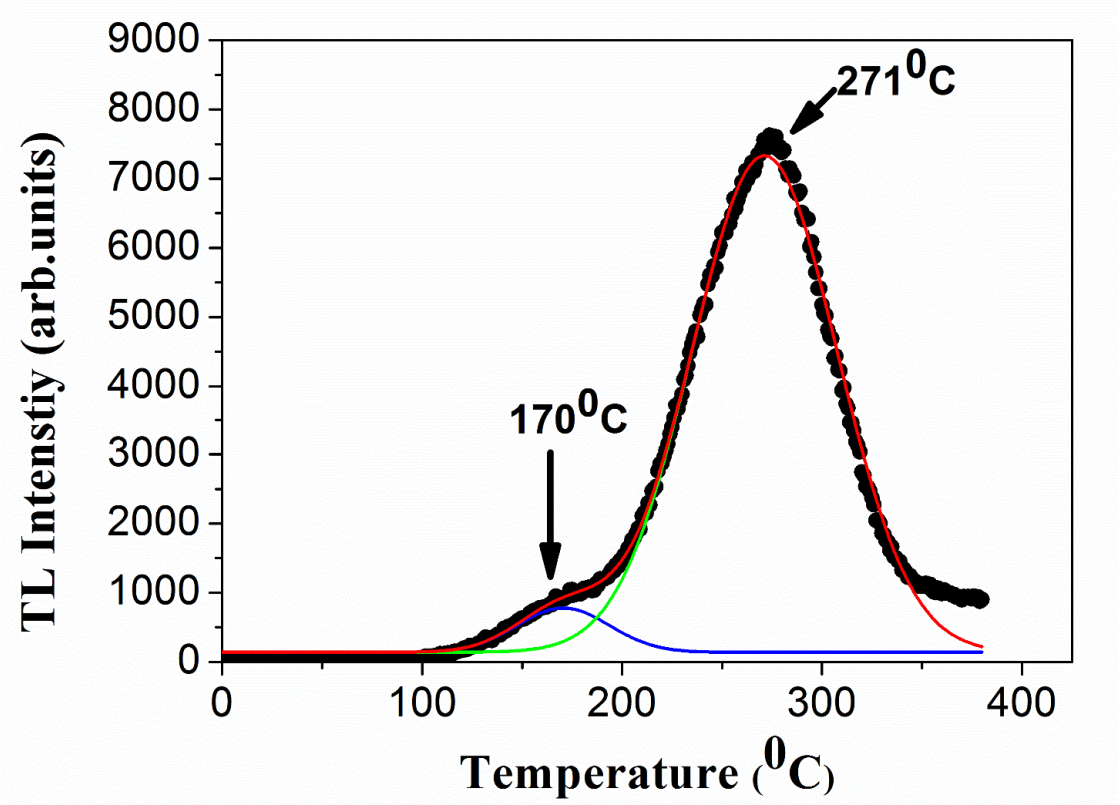

Figure 10. Thermo-luminescence spectrum of the grown CNTAO single crystal.

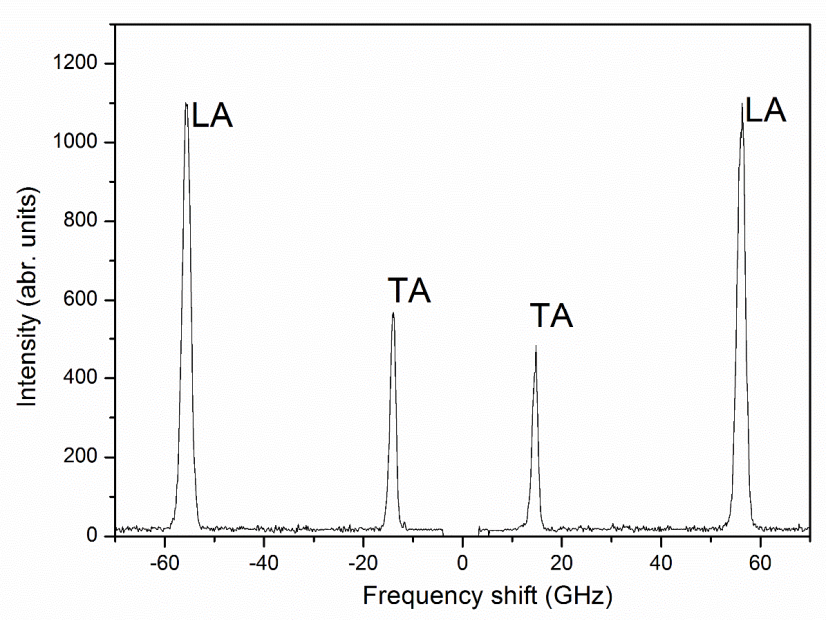

Figure 11. Brillouin spectrum of CNTAO single crystal measured at room temperature.